Raising the Bar: Increased Hydraulic Pressure Allows Unprecedented High Power Densities in Pressure-Retarded Osmosis

ARTICLE · NOVEMBER 2013

DOI: 10.1021/ez400117d

3 AUTHORS, INCLUDING:

Anthony P. Straub
Yale University
11 PUBLICATIONS **164** CITATIONS
SEE PROFILE

Menachem Elimelech
Yale University
394 PUBLICATIONS **32,554** CITATIONS
SEE PROFILE

Environmental Science & Technology Letters

Letter

pubs.acs.org/journal/estlcu

Raising the Bar: Increased Hydraulic Pressure Allows Unprecedented High Power Densities in Pressure-Retarded Osmosis

Anthony P. Straub, Ngai Yin Yip, and Menachem Elimelech*

Department of Chemical and Environmental Engineering, Yale University, New Haven, Connecticut 06520-8286, United States

Supporting Information

ABSTRACT: Pressure-retarded osmosis (PRO) has the potential to generate sustainable energy from salinity gradients. PRO is typically considered for operation with river water and seawater, but a far greater energy of mixing can be harnessed from hypersaline solutions. This study investigates the power density that can be obtained in PRO from such concentrated solutions. Thin-film composite membranes with an embedded woven mesh were supported by tricot fabric feed spacers in a specially designed crossflow cell to maximize the operating pressure of the system, reaching a stable applied hydraulic pressure of 48 bar (700 psi) for more than 10 h. Operation at this increased hydraulic pressure allowed unprecedented power densities, up to 60 W/m^2 with a 3 M (180 g/L) NaCl draw solution. Experimental power densities demonstrate reasonable agreement with power densities modeled using measured membrane properties, indicating high-pressure operation does not drastically alter membrane performance. Our findings exhibit the promise of the generation of power from high-pressure PRO with concentrated solutions.

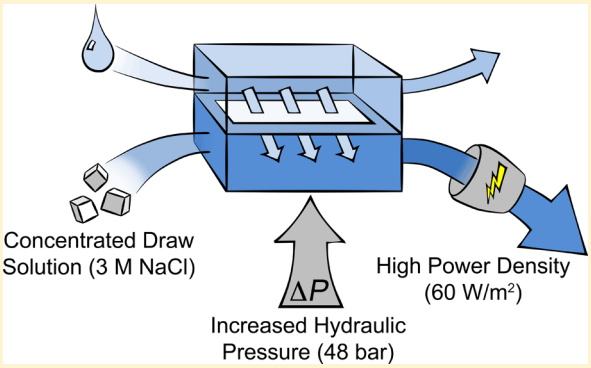

INTRODUCTION

Natural and anthropogenic salinity gradients have been identified as significant sources of sustainable energy that are currently untapped.[1,2] The Gibbs free energy released during mixing can be harnessed by technologies such as reverse electrodialysis,[3,4] capacitive mixing,[5] and pressure-retarded osmosis (PRO).[6,7] In PRO, a semipermeable membrane separates a low-concentration feed solution from a high-concentration draw solution. The osmotic pressure difference between the two solutions drives a pressurized flow of water from the feed to the draw solution, which then generates electricity by a hydroturbine.

PRO studies have mainly focused on capturing the energy released when fresh river water meets the sea.[8−11] However, more concentrated solutions capable of producing greater energy have also been suggested for use in PRO since the 1970s.[6,12,13] In locations where fresh water naturally flows into hypersaline water bodies, such as the Dead Sea and the Great Salt Lake, the theoretical energy of mixing released is nearly 20 times larger than that at river water−seawater interfaces.[1] Other anthropogenic hypersaline sources, such as brines from salt dome mining[12] or water produced from hydraulic fracturing,[14] also have the potential to generate power in a controlled mixing process. Alternatively, PRO can be applied in a closed-loop heat engine, where synthetic draw solutions are separated and regenerated using low-grade heat.[1,15] Such systems employ highly concentrated working solutions to exploit large mixing energies.

Higher-concentration streams have enormous potential in PRO as they are capable of producing greatly enhanced power density, defined as the power generated per unit membrane area, a critical factor in determining the economic viability of a PRO plant.[9,16] However, to access the high-power density potential of concentrated solutions, the PRO system, including the membranes, must be able to withstand a hydraulic pressure that is approximately half the osmotic pressure of the concentrated draw solution. In the case of a 2 M (120 g/L) NaCl draw solution, the system should be operated at ∼50 bar (725 psi), nearly equivalent to the applied pressure of a seawater reverse osmosis (RO) desalination plant.[17] In literature, the highest PRO operating pressure reported is 24 bar,[18] with most studies reaching only ∼16 bar before membrane damage or system limitations prevent further pressurization.[19−21] Thus, the potential for high-power density PRO remains unrealized.

In this study, we conduct an experimental analysis of PRO performance using concentrated NaCl draw solutions and demonstrate unprecedented high power densities (up to 60 W/m^2) at elevated hydraulic pressure difference. The PRO system channel, spacer, and membrane were carefully designed to allow PRO operation at high applied hydraulic pressures (up to 48 bar or 700 psi). Experimental power densities are compared

Received: October 17, 2013
Revised: November 10, 2013
Accepted: November 11, 2013
Published: November 11, 2013

   dx.doi.org/10.1021/ez400117d | Environ. Sci. Technol. Lett. 2014, 1, 55−59

to power densities modeled from experimentally determined membrane properties to evaluate the potential of PRO using highly concentrated draw solutions.

MATERIALS AND METHODS

Membrane and Spacers. Commercial flat-sheet, thin-film composite (TFC) forward osmosis (FO) membranes were obtained from Hydration Technology Innovations (Albany, OR). Membranes were loaded into a specially designed crossflow test cell and oriented with the active layer facing the concentrated draw solution and the support layer facing the dilute feed solution. In the feed channel, two layers of tricot woven fabric were used to support the membrane under pressure and maintain the channel geometry. In the draw channel, a biplanar extruded netting spacer was employed to induce turbulence and support the membrane. Images of both spacer types are shown in Figure S1 of the Supporting Information. Scanning electron microscopy (SEM) characterization of membranes and spacers is also described in the Supporting Information.

Bench-Scale Experimental PRO Setup. A diagram of the custom-built crossflow test cell is shown in Figure 1. The feed and draw channel heights are 0.5 and 1 mm, respectively, similar to the dimensions of a spiral wound membrane element.[22] Both channels were 10.7 cm long and 3.6 cm wide. The edges of each membrane coupon were covered with water-resistant tape such that only a 7.7 cm × 2.6 cm portion of the membrane was exposed. This design prevented deformation of the membrane on the edges of the channel and allowed more uniform flow conditions across the exposed membrane. The feed channel inlet and outlet comprise parallel slit openings (1 mm wide each) to further prevent membrane deformation and rupture. The bench-scale experimental setup is shown in Figure S2 of the Supporting Information, and details of the setup are described in the Supporting Information.

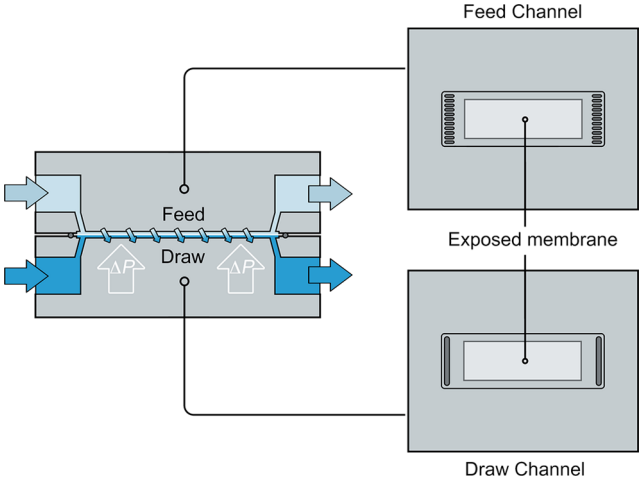

Figure 1. Schematic diagram of the specially designed laboratory-scale crossflow membrane test cell. The feed channel height is 0.5 mm, and the draw channel height is 1 mm. Both channels are 10.7 cm long and 3.6 cm wide, with a 7.7 cm × 2.6 cm exposed membrane area. The feed channel is fabricated with thin, parallel openings.

PRO Experimental Protocol. Membranes were first compacted by circulating deionized (DI) water on both sides of the membrane and gradually increasing the applied hydraulic pressure on the draw side of the membrane (i.e., the active layer side). Once the maximal intended applied pressure for a given experiment was reached, the membrane was allowed to equilibrate for at least 10 h, with water permeating from the draw side to the feed side of the membrane because of the hydraulic pressure difference, ΔP. After compaction, the stable DI water flux was recorded. A concentrated NaCl stock solution was then dosed to the solution on the draw (active layer) side of the membrane to increase the concentration to 50 mM. At this concentration, ΔP still exceeds the osmotic pressure difference. Hence, water continues to permeate from the pressured draw side to the feed side of the membrane, although at a reduced rate. The stabilized water and salt flux measurements were taken over a 20 min duration and used, along with the aforementioned DI water flux, to determine the mass transfer coefficient at the draw–membrane interface, k, and verify the selectivity of the membrane. Details of the full procedure are given in the Supporting Information.

To initiate PRO operation, a concentrated NaCl stock solution was added to the draw solution to achieve the desired concentration (0.6, 1, 2, or 3 M NaCl). Under this condition, the draw solution osmotic pressure exceeds the applied hydraulic pressure and the water flux direction is reversed, permeating from the feed into the draw side. The system was allowed to stabilize for 15 min before the water flux was recorded over 20 min. The pressure was then decreased stepwise, and stable water flux measurements were recorded at each step. All experiments were performed in duplicate with a different membrane sample at 25 ± 0.5 °C.

Power Density Calculation. The membrane power density, W, is defined as the power generated per unit membrane area and is the product of the PRO water flux, J_w, and the corresponding applied hydraulic pressure, ΔP:

$$W = J_w \Delta P \tag{1}$$

The power densities calculated from the experimentally determined water fluxes (eq 1) were compared to power densities predicted with membrane parameters determined in an RO and FO membrane characterization, where the water permeability, A, and salt permeability, B, are determined using RO water flux and salt rejection measurements and the structural parameter, S, is determined from an FO water flux measurement.[23] Details of this characterization method can be found in the Supporting Information.

The predicted water flux was calculated using

$$J_w = A(\pi_{D,m} - \pi_{F,m} - \Delta P) \tag{2}$$

where the osmotic pressures at the active layer interface on the draw and feed sides ($\pi_{D,m}$ and $\pi_{F,m}$, respectively) are determined using results from commercial software from OLI Systems (Morris Plains, NJ) and calculated concentrations at the membrane active layer interface. The third-order polynomial equation used to calculate osmotic pressure, which was determined from OLI data, is presented in Figure S3 of the Supporting Information. This equation accounts for the nonlinear dependence of osmotic pressure on molar concentration that is exacerbated at the high salt concentrations explored in this investigation. The effects of internal concentration polarization, external concentration polarization, and reverse salt permeation were taken into account when determining the concentrations at the active layer interface of the draw and feed sides ($c_{D,m}$ and $c_{F,m}$, respectively):[11]

$$c_{D,m} = c_{D,b}\exp\left(-\frac{J_w}{k}\right) - \frac{B}{J_w}(c_{D,m} - c_{F,m})\left[1 - \exp\left(-\frac{J_w}{k}\right)\right] \quad (3)$$

$$c_{F,m} = c_{F,b}\exp\left(\frac{J_w S}{D}\right) + \frac{B}{J_w}(c_{D,m} - c_{F,m})\left[\exp\left(\frac{J_w S}{D}\right) - 1\right] \quad (4)$$

where $c_{D,b}$ and $c_{F,b}$ are the draw and feed solution bulk concentrations, respectively, and the NaCl diffusion coefficient, D, is assumed to be 1.48×10^{-9} m^2/s.[24]

RESULTS AND DISCUSSION

The Membrane and Spacer Design Is Critical for High-Pressure Operation. A critical parameter in PRO is the burst pressure, defined as the hydraulic pressure applied to the draw solution at which the integrity of the membrane active layer is compromised. To determine the burst pressure, the draw solution hydraulic pressure was increased in 6.9 bar (100 psi) increments and the water flux with DI water feed was monitored. Throughout the tests, the pure water flux was found to remain stable at 48.3 bar (700 psi), indicating the membrane active layer was not compromised. However, when ΔP was increased to 55.2 bar (800 psi), replicate membranes loaded in the test cell exhibited a rapid increase in water flux to more than double the expected value within 15 min, indicating failure of the active layer (i.e., the burst pressure is between 48.3 and 55.2 bar). The applied pressure of 48.3 bar (700 psi), which was maintained for more than 10 h in repeated experiments, is considerably greater than the highest reported operating pressure for flat-sheet or hollow fiber PRO membranes (16.7 and 23.8 bar, respectively).[18,25]

The substantially increased burst pressure is attributed to the membrane, spacer, and channel design (Figures 1 and 2). During pressurization, the active layer of the membrane is forced against the support layer, which rests on the feed spacer and channel (Figure 2D). For high-pressure operation, it is critical that all of these components minimize deformation of the active layer.

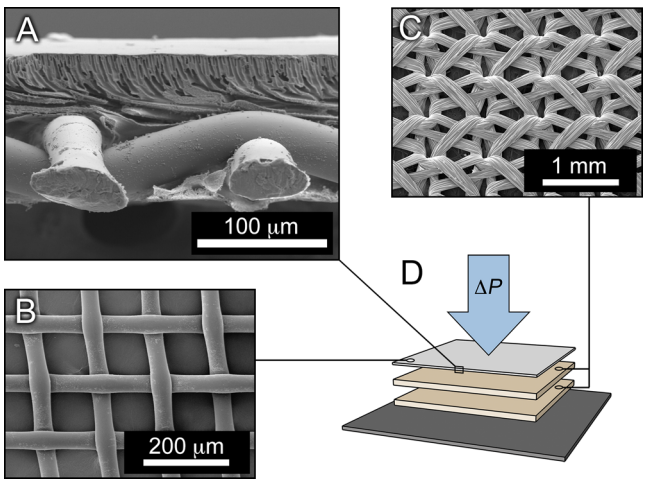

Figure 2. SEM micrographs displaying (A) the pristine HTI thin-film composite (TFC) membrane cross section, (B) the polyester mesh embedded in the support layer of the membrane, and (C) the tricot fabric feed channel spacer. (D) During operation, the applied hydraulic pressure difference, ΔP, compresses the membrane active layer against the support layer, two sheets of tricot fabric, and the feed channel wall.

Figure 2A shows an SEM image of the pristine TFC membrane cross section, with a total membrane thickness of ~115 μm. The unique polyester mesh embedded in the support layer of the TFC membrane is also clearly visible in the cross section. Figure 2B shows a top-down view of the woven mesh only (the polysulfone porous layer was dissolved with a dimethylformamide solvent), with ~150 μm spacing between each 40 μm wide fiber. We postulate that the fine mesh reinforced the porous polysulfone support layer by evenly distributing the load, thus strengthening the composite membrane. In addition, the fingerlike macrovoids spanning the thickness of the polysulfone support layer have been shown to minimize the detrimental effects of internal concentration polarization on water flux.[11,26]

The feed channel spacer must be designed to further prevent membrane deformation. Tricot woven fabric, the material used in this study, is widely employed in commercial seawater reverse osmosis membrane modules and was also used previously in an experimental PRO spiral-wound module.[22] SEM images of the fabric (Figure 2C) demonstrate relatively small openings, with the largest unsupported gap being approximately 350 μm wide, much smaller than the openings of plastic webbed spacers used in previous PRO tests.[20,27] We propose the tight weave provided a robust scaffold structure that helped suppress membrane deformation.

Similarly, we specially designed the crossflow channel to support the membrane under high pressure. Feed channel inlets and outlets were outfitted with 1 mm slits that prevented the membrane from folding and rupturing under high pressure (Figure 1). Water-resistant tape was also used to prevent rupture of the membrane on the edges of the channel. The careful design of the channel, along with the aforementioned selection of membrane and feed spacer design, allowed PRO experiments to reach the unprecedented high pressures.

High Power Densities Are Realized at Elevated Pressures and Draw Solution Concentrations. Experimental power densities determined from eq 1 are presented in Figure 3 (blue circles and red squares), and numerical values for water flux and power density are listed in Table S1 of the Supporting Information. The 0.6 and 1 M NaCl draw solutions are representative of seawater and brine from seawater RO desalination, respectively, while 2 and 3 M NaCl draw solutions were employed to model hypersaline water sources or synthetic draw solutions in a closed-loop osmotic heat engine.[1] Maximal power densities of 7.5, 14.1, 39.4, and 59.7 W/m^2 were achieved for the 0.6, 1, 2, and 3 M NaCl draw solutions, respectively. The corresponding applied hydraulic pressures were 13.8, 20.7, 41.4, and 48.3 bar, respectively. Peak power density results for 0.6 and 1 M draw solutions were comparable to those previously obtained using other TFC membranes.[16,19,28] The methodical design of the PRO setup allowed the experiments to operate near the peak power density of the 2 and 3 M NaCl draw solutions, a pivotal condition that constrained past studies,[20,29] thus yielding unmatched power densities.

The membrane transport properties were determined and used to model the expected performance. In an RO crossflow test cell, the HTI-TFC membrane demonstrated an average water permeability coefficient, A, of 2.49 L m^{-2} h^{-1} bar^{-1} and a salt (NaCl) permeability coefficient, B, of 0.39 L m^{-2} h^{-1}. These values of A and B are typical for membranes with a

dx.doi.org/10.1021/ez400117d | Environ. Sci. Technol. Lett. 2014, 1, 55−59

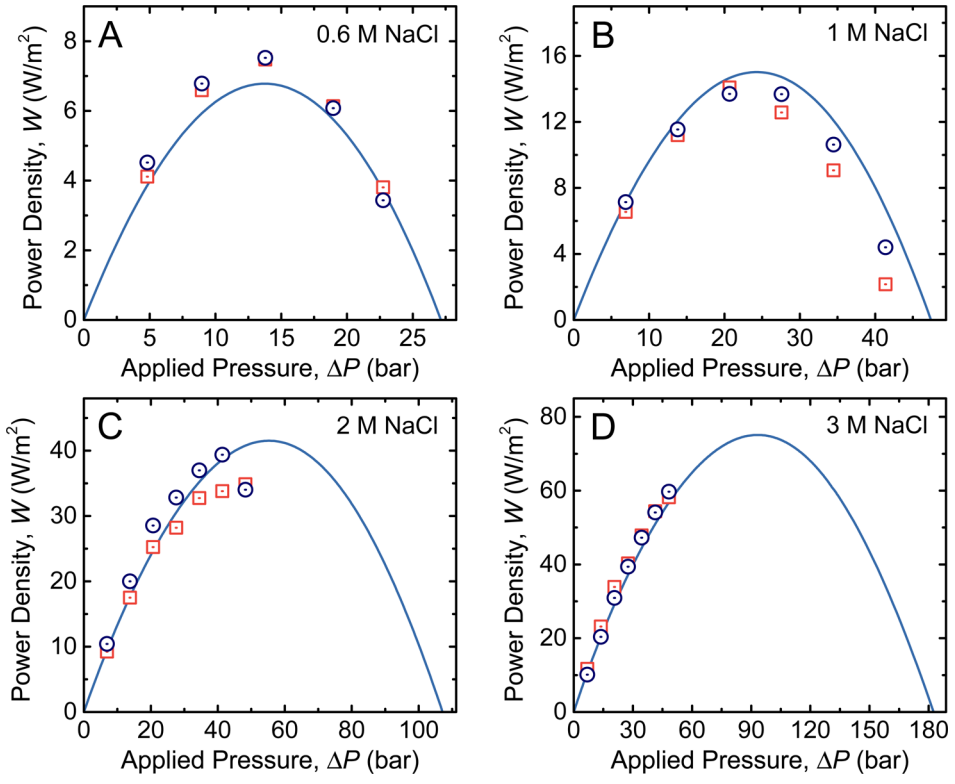

Figure 3. Experimental and modeled projected power densities as a function of applied hydraulic pressure difference, ΔP. Draw (NaCl) solution concentrations of (A) 0.6, (B) 1, (C) 2, and (D) 3 M were used with osmotic pressures of 28.3, 49.4, 111.2, and 188.8 bar, respectively (calculated using OLI software). Modeled power densities (light blue lines) were determined using parameters from an RO and FO characterization. Experimental power densities were determined in duplicate using eq 1 (blue circles and red squares). All experiments were performed with feed (DI water) and draw solutions at 25 ± 0.5 °C.

polyamide active layer.[30,31] The structural parameter, S, was determined to be 564 μm using water flux measurements from an FO test.[23,26] The average feed mass transfer coefficient, k, was calculated to be 27.5 μm/s (99 L m^{-2} h^{-1}) using measurements in the PRO channel.

Predicted power densities using the determined A, B, S, and k values, eqs 1−4, and osmotic pressures from OLI are presented in Figure 3 (light blue lines). The model results are in reasonable agreement with experimental data. This is in contrast to several previous publications, where membrane deformation or spacer shadow effect led to a lower-than-expected power density.[18,20,29] In fact, the experimental power density was slightly higher than the predicted values for some of the experiments. This observation can be attributed to differences in the actual membrane properties during PRO operation and those determined in the RO and FO characterization. For example, the water permeability of the membrane may increase because of slight deformation,[20] or the structural parameter may decrease because of a reduction in the thickness of the support layer.

High-Pressure PRO Holds Promise as an Economical Means of Salinity Gradient Power Generation. This study demonstrates that proper membrane, spacer, and flow channel design allows PRO operation at substantially increased hydraulic pressures, thus allowing the high-power density potential of concentrated draw solutions to be accessed. The ability to obtain such high power densities using commercially available membranes is a considerable step toward the adoption of PRO as a viable technology for harvesting salinity energy, because the initial membrane cost will define much of the capital cost of a PRO plant.[9] For processes such as the closed-loop osmotic heat engine, which uses PRO and concentrated synthetic solutions to harness the energy available in low-grade heat,[1,15] an increase in the achievable power density is essential for the practicality of the system.

To further advance the technology, development of mechanically robust, high-flux membrane modules customized for high-pressure PRO is necessary. The effect of the decrease in axial pressure along the feed channel and reverse salt flux have been identified as key factors that can detrimentally affect PRO productivity in a full-scale module and, thus, warrant further study.[18,22] Furthermore, an extensive economic evaluation should consider the cost of treating or producing a suitably concentrated draw solution. With the performance demonstrated in this study and further technological improvements, high-pressure PRO may be realized as a commercially feasible method for harnessing the renewable energy stored in salinity gradients.

■ ASSOCIATED CONTENT

Supporting Information

Details of the SEM imaging technique, an explanation of the bench-scale experimental setup, methods for determining the feed solution mass transfer coefficient and membrane selectivity in the PRO channel, characterization method for determining intrinsic membrane properties using FO and RO measurements, a complete set of experimental water flux and power density measurements (Table S1), images of the feed and draw channel spacers (Figure S1), a schematic diagram of the bench-scale PRO experimental setup (Figure S2), and the osmotic

pressure equation used in modeling (Figure S3). This material is available free of charge via the Internet at http://pubs.acs.org.

AUTHOR INFORMATION

Corresponding Author

*E-mail: menachem.elimelech@yale.edu. Phone: (203) 432-2789.

Notes

The authors declare no competing financial interest.

ACKNOWLEDGMENTS

We acknowledge the support received from the National Science Foundation under Award Number CBET 1232619 and from the Advanced Research Projects Agency-Energy (ARPA-E), U.S. Department of Energy, via Grant DE-AR0000306. We also acknowledge the National Science Foundation Graduate Research Fellowship awarded to A.P.S. and the Graduate Fellowship (N.Y.Y.) made by the Environment and Water Industrial Development Council of Singapore.

REFERENCES

(1) Logan, B. E.; Elimelech, M. Membrane-based processes for sustainable power generation using water. *Nature* **2012**, *488*, 313−319.

(2) Pattle, R. E. Production of electric power by mixing fresh and salt water in the hydroelectric pile. *Nature* **1954**, *174*, 660.

(3) Post, J. W.; Hamelers, H. V. M.; Buisman, C. J. N. Energy recovery from controlled mixing salt and fresh water with a reverse electrodialysis system. *Environ. Sci. Technol.* **2008**, *42*, 5785−5790.

(4) Długołęçki, P.; Gambier, A.; Nijmeijer, K.; Wessling, M. Practical potential of reverse electrodialysis as process for sustainable energy generation. *Environ. Sci. Technol.* **2009**, *43*, 6888−6894.

(5) Brogioli, D. Extracting Renewable Energy from a Salinity Difference Using a Capacitor. *Phys. Rev. Lett.* **2009**, *103*, 058501.

(6) Loeb, S. Osmotic power plants. *Science* **1975**, *189*, 654−655.

(7) Achilli, A.; Childress, A. E. Pressure retarded osmosis: From the vision of Sidney Loeb to the first prototype installation: Review. *Desalination* **2010**, *261*, 205−211.

(8) Ramon, G. Z.; Feinberg, B. J.; Hoek, E. M. V. Membrane-based production of salinity-gradient power. *Energy Environ. Sci.* **2011**, *4*, 4423−4434.

(9) Skilhagen, S. E. Osmotic power: A new, renewable energy source. *Desalin. Water Treat.* **2010**, *15*, 271−278.

(10) Thorsen, T.; Holt, T. The potential for power production from salinity gradients by pressure retarded osmosis. *J. Membr. Sci.* **2009**, *335*, 103−110.

(11) Yip, N. Y.; Tiraferri, A.; Phillip, W. A.; Schiffman, J. D.; Hoover, L. A.; Kim, Y. C.; Elimelech, M. Thin-film composite pressure retarded osmosis membranes for sustainable power generation from salinity gradients. *Environ. Sci. Technol.* **2011**, *45*, 4360−4369.

(12) Wick, G.; Isaacs, J. Salt domes: Is there more energy available from their salt than from their oil? *Science* **1978**, *199*, 1436−1437.

(13) Loeb, S. Production of energy from concentrated brines by pressure-retarded osmosis. I. Preliminary technical and economic correlations. *J. Membr. Sci.* **1976**, *1*, 49−63.

(14) Shaffer, D. L.; Arias Chavez, L. H.; Ben-Sasson, M.; Romero-Vargas Castrillón, S.; Yip, N. Y.; Elimelech, M. Desalination and reuse of high-salinity shale gas produced water: Drivers, technologies, and future directions. *Environ. Sci. Technol.* **2013**, *47*, 9569−9583.

(15) McGinnis, R. L.; McCutcheon, J. R.; Elimelech, M. A novel ammonia−carbon dioxide osmotic heat engine for power generation. *J. Membr. Sci.* **2007**, *305*, 13−19.

(16) Gerstandt, K.; Peinemann, K. V.; Skilhagen, S. E.; Thorsen, T.; Holt, T. Membrane processes in energy supply for an osmotic power plant. *Desalination* **2008**, *224*, 64−70.

(17) Fritzmann, C.; Löwenberg, J.; Wintgens, T.; Melin, T. State-of-the-art of reverse osmosis desalination. *Desalination* **2007**, *216*, 1−76.

(18) Zhang, S.; Chung, T. S. Minimizing the instant and accumulative effects of salt permeability to sustain ultrahigh osmotic power density. *Environ. Sci. Technol.* **2013**, *47*, 10085−10092.

(19) Chou, S.; Wang, R.; Fane, A. G. Robust and high performance hollow fiber membranes for energy harvesting from salinity gradients by pressure retarded osmosis. *J. Membr. Sci.* **2013**, *448*, 44−54.

(20) Kim, Y. C.; Elimelech, M. Adverse impact of feed channel spacers on the performance of pressure retarded osmosis. *Environ. Sci. Technol.* **2012**, *46*, 4673−4681.

(21) Song, X.; Liu, Z.; Sun, D. D. Energy recovery from concentrated seawater brine by thin-film nanofiber composite pressure retarded osmosis membranes with high power density. *Energy Environ. Sci.* **2013**, *6*, 1199−1210.

(22) Kim, Y. C.; Kim, Y.; Oh, D.; Lee, K. H. Experimental Investigation of a Spiral-Wound Pressure-Retarded Osmosis Membrane Module for Osmotic Power Generation. *Environ. Sci. Technol.* **2013**, *47*, 2966−2973.

(23) Yip, N. Y.; Tiraferri, A.; Phillip, W. A.; Shiffman, J. D.; Elimelech, M. High performance thin-film composite forward osmosis membrane. *Environ. Sci. Technol.* **2010**, *44*, 3812−3818.

(24) Vitagliano, V.; Lyons, P. A. Diffusion coefficients for aqueous solutions of sodium chloride and barium chloride. *J. Am. Chem. Soc.* **1956**, *78*, 1549−1552.

(25) Han, G.; Wang, P.; Chung, T. S. Highly Robust Thin-Film Composite Pressure Retarded Osmosis (PRO) Hollow Fiber Membranes with High Power Densities for Renewable Salinity-Gradient Energy Generation. *Environ. Sci. Technol.* **2013**, *47*, 8070−8077.

(26) Tiraferri, A.; Yip, N. Y.; Phillip, W. A.; Schiffman, J. D.; Elimelech, M. Relating performance of thin-film composite forward osmosis membranes to support layer formation and structure. *J. Membr. Sci.* **2011**, *367*, 340−352.

(27) Achilli, A.; Cath, T. Y.; Childress, A. E. Power generation with pressure retarded osmosis: An experimental and theoretical investigation. *J. Membr. Sci.* **2009**, *343*, 42−52.

(28) Han, G.; Zhang, S.; Li, X.; Chung, T. S. High performance thin film composite pressure retarded osmosis (PRO) membranes for renewable salinity-gradient energy generation. *J. Membr. Sci.* **2013**, *440*, 108−121.

(29) She, Q.; Jin, X.; Tang, C. Y. Osmotic power production from salinity gradient resource by pressure retarded osmosis: Effects of operating conditions and reverse solute diffusion. *J. Membr. Sci.* **2012**, *401−402*, 262−273.

(30) Yip, N. Y.; Elimelech, M. Performance limiting effects in power generation from salinity gradients by pressure retarded osmosis. *Environ. Sci. Technol.* **2011**, *45*, 10273−10282.

(31) Tiraferri, A.; Yip, N. Y.; Straub, A. P.; Romero-Vargas Castrillón, S.; Elimelech, M. A Method for the Simultaneous Determination of Transport and Structural Parameters of Forward Osmosis Membranes. *J. Membr. Sci.* **2013**, *444*, 523−538.